Noise Figure of Vertical-Cavity Semiconductor Optical Amplifiers

E. Staffan Björlin, *Student Member, IEEE,* and John E. Bowers, *Fellow, IEEE*

***Abstract*—The noise figure of vertical-cavity semiconductor optical amplifiers(VCSOAs) is investigated theoretically and experimentally. Limitations on the noise figure set by the reflectivity of the mirrors are studied. Highly reflective mirrors lead to increased output noise as well as lasing at moderate carrier densities, which imposes a limit on the obtainable population inversion. Expressions for the excess noise coefficient, which governs signal-spontaneous beat noise enhancement due to finite mirror reflectivity, are presented for transmission and reflection-mode operation. Experimental results from a VCSOA operating in the reflection mode at 1.3 μm are presented. The results, from optical as well as electrical measurement techniques, are analyzed and compared to theoretical values.**

***Index Terms*—Amplifier noise, laser amplifiers, noise, noise measurement, optical noise, semiconductor optical amplifiers.**

I. Introduction

VERTICAL-CAVITY semiconductor optical amplifiers (VCSOAs) are interesting devices for a wide range of applications in optical communication systems. The vertical-cavity design gives these devices a number of advantages over in-plane devices, such as high coupling efficiency to optical fiber, low power consumption, small form factor, and the possibility of fabricating 2-D arrays on wafer. Furthermore, the technology allows for on-wafer testing and is compatible with low-cost manufacturing and packaging techniques. These advantages all draw from the fundamental geometrical differences between the vertical cavity and the in-plane designs. In a vertical-cavity structure, the optical mode passes perpendicularly through the different material layers. Consequently, the electrical field is always parallel to the plane of the active layers. This makes VCSOAs insensitive to the polarization of the signal light. It also makes the gain per pass very small, on the order of a few percent. VCSOAs, therefore, use feedback provided by high reflectivity distributed Bragg reflector (DBR) mirrors. The feedback constricts the gain bandwidth to the linewidth of the Fabry–Perot mode, which essentially limits the operation to amplification of a single signal. The narrow bandwidth also filters out out-of-band noise, making VCSOAs ideal as preamplifiers in receiver modules. The vertical cavity is circularly symmetric around the axis perpendicular to the two mirrors and naturally supports a circular optical mode. This yields high coupling efficiency to optical fiber, which is beneficial for achieving a low noise figure.

VCSOAs operating at all important telecommunication wavelengths have been demonstrated. Room-temperature continuous-wave (CW) operation was demonstrated at 980 [1] and 1300 nm [2]. CW operation at 217 K [3] and pulsed operation at room temperature [4] were demonstrated at 1550 nm. These papers present experimental results for gain, gain bandwidth, and saturation power. VCSOAs have also been examined theoretically [5]–[7]. Models based on rate equations and/or Fabry–Perot models have been developed to predict performance and aid device design.

Optical amplifiers are incorporated into optical communication systems in order to increase transmission distance or receiver sensitivity. However, amplification is achieved at the cost of compromised signal integrity. This is due to the fact that amplification of an optical signal also adds undesired power fluctuations to the signal. These power fluctuations are unavoidable as they are inherent to the randomness of the amplification process. The power fluctuations degrade the signal-to-noise ratio (SNR), ultimately leading to undetectable information. The noise figure is a figure of merit for the SNR degradation, and hence for the power penalty associated with the introduction of the device into a transmission system. This makes the noise figure one of the most important properties of optical amplifiers for their applications in optical communication systems. The noise figure of optical amplifiers has been extensively studied [8]–[15]. Fiber amplifiers—as well as both traveling wave (TW) and Fabry–Perot (FP) in-plane SOAs—have been investigated, but the particular case of VCSOAs has been only briefly studied [2], [5]. This paper presents theory, as well as experimental results, for the noise figure of VCSOAs. The theory is based on previous work on FP in-plane SOAs. It describes how the typically high reflectivity of the VCSOA mirrors affects the output noise and what limitations it sets to the obtainable noise figure. Operation in transmission mode, as well as reflection mode, is covered. Noise-figure degradation caused by coupling losses is also examined. Experimental results for the noise figure of an optically pumped 1.3-μm VCSOA operated in reflection mode are presented. Electrical methods, as well as optical methods, were used in the noise figure measurements. The experimental and theoretical results are compared and show good agreement.

II. Theory

Several different approaches have been used to describe noise in optical amplifiers, either quantum mechanical or semiclassical [8], [9]. Noise in SOAs has been analyzed using

Manuscript received June 29, 2001; revised October 5, 2001. This work was supported by the Defense Advanced Research Projects Agency (DARPA), via the Center for Chips with Heterogeneously Integrated Photonics (CHIPS).

The authors are with the University of California, Santa Barbara, Electrical and Computer Engineering Department, Santa Barbara, CA 93106 USA (e-mail: bjorlin@ece.ucsb.edu).

Publisher Item Identifier S 0018-9197(02)00169-0.

0018–9197/02$17.00 © 2002 IEEE

rate equations [10], as well as photon statistics master equations [10]–[13]. Traveling wave equations have been used in order to take the spatial distribution of carriers, gain, and photons in in-plane SOAs into account [14]. In a VCSOA, the gain is concentrated to an extremely small gain region. The signal traverses the gain region multiple times and experiences the same gain each time. The traveling wave approach is therefore not necessary for this case. However, VCSOAs typically have highly reflective mirrors, which greatly affects the noise properties. The noise in VCSOAs can be analyzed using the same methods as for in-plane FPAs. The total output noise from an optical amplifier consists of several different noise terms of different origin. The terms contributing to the total noise are: beating between amplified spontaneous emission (ASE) components and the coherent signal light, beating between different ASE components, and shot noise due to both signal and ASE. The input signal might also have some excess noise and the receiver adds thermal noise. Signal-spontaneous beat noise is independent of the input signal power and is the dominating term at low signal power. This term depends on the optical bandwidth of the ASE spectrum. For this reason, a bandpass filter is normally used after the optical amplifier in order to minimize the amount of ASE reaching the detector. This is not needed for a VCSOA as the spontaneous emission bandwidth is limited by the Fabry–Perot cavity. Signal-spontaneous beat noise and shot noise increase with input signal power. At high signal powers, signal-spontaneous beat noise is the main contributor to the output noise. The output ASE, and hence the signal-spontaneous beat noise, is greatly affected by the mirror reflectivity. Considering signal-spontaneous beat noise to be dominant, the noise factor F, defined as input SNR over output SNR (the noise *figure* is defined as $NF = 10\log(F)$ and expressed in decibels), is given by $F = 2n_{\rm sp}\chi(G-1)/G$ [15]. For high signal gain ($G \gg 1$), this reduces to

$$F = 2n_{\rm sp}\chi. \tag{1}$$

Here, $n_{\rm sp}$ is the population inversion parameter and χ is the excess noise coefficient, which describes signal-spontaneous beat noise enhancement due to finite mirror reflectivity. χ takes on a value of one for zero reflectivity (the case of traveling wave amplifiers) and values higher than one for finite mirror reflectivities. Using photon statistics master equations as described by Shimoda *et al.* [11], it can be shown that χ is given by [12]

$$\chi = \frac{(1+R_b g_s)(1-R_t)(g_s-1)}{\left(1-\sqrt{R_t R_b}g_s\right)(G-1)} \tag{2}$$

where

- R_b bottom mirror reflectivity;
- R_t top mirror reflectivity;
- g_s single-pass gain;
- G amplifier gain.

Here, the signal is exiting the amplifier through the top mirror. VCSOAs can be operated in either transmission or reflection mode with different expressions for the signal gain G. Since G appears in the denominator of (2), the two configurations are associated with significantly different expressions for χ. In transmission-mode operation, the signal enters the VCSOA from one side (bottom) and is collected on the other side (top). In reflection mode, the signal enters and exits the amplifier from the same side (top). The amplifier gain of a VCSOA operated in transmission mode (G_t) or reflection mode (G_r) is given by [5]

$$G_t = \frac{(1-R_t)(1-R_b)g_s}{\left(1-\sqrt{R_t R_b}g_s\right)^2 + 4\sqrt{R_t R_b}g_s\sin^2\varphi} \tag{3}$$

$$G_r = \frac{\left(\sqrt{R_t}-\sqrt{R_b}g_s\right)^2 + 4\sqrt{R_t R_b}g_s\sin^2\varphi}{\left(1-\sqrt{R_t R_b}g_s\right)^2 + 4\sqrt{R_t R_b}g_s\sin^2\varphi}. \tag{4}$$

Here, φ is the phase detuning off the cavity resonance frequency. For operation at the cavity resonance frequency, the sine terms equal zero. Inserting (3) and (4) back into (2), the excess noise coefficient for the two cases can be shown to be

$$\chi_t = \frac{(1+R_b g_s)(1-R_t)(g_s-1)}{(1-R_b)(1-R_t)g_s - \left(1-\sqrt{R_t R_b}g_s\right)^2} \tag{5}$$

$$\chi_r = \frac{(1+R_b g_s)(g_s-1)}{(R_b g_s^2-1)}. \tag{6}$$

For transmission mode and high gain ($G \gg 1$), χ simplifies to

$$\chi_t = \frac{(1+R_b g_s)(g_s-1)}{(1-R_b)g_s}. \tag{7}$$

The excess noise coefficient versus amplifier gain for both cases is plotted in Fig. 1(a) and (b), for different mirror reflectivities. The reflectivity of VCSOA mirrors is typically much higher than for those of in-plane FP amplifiers due to the shorter active region of VCSOAs and, thereby, lower single-pass gain. VCSOAs demonstrated to date have all used mirrors with reflectivities higher than 0.9. χ is shown here for mirror reflectivities of 0.85 and higher. For transmission-mode operation [Fig. 1(a)], χ_t equals one when the single-pass gain is $g_s = R_b^{-1/2}$. It is obviously desirable to operate the VCSOA close to this ideal value of g_s, but at the same time be able to vary the signal gain G. It is also desirable to maximize g_s in order to achieve high signal gain. This can be achieved by using low input mirror reflectivity (R_b) and high output mirror reflectivity (R_t). This is evident from Fig. 1(a); a value of χ_t close to one over a wide range of signal gain is achieved using $R_b = 0.85$ and $R_t = 0.95$. For symmetrical devices, χ_t is independent of mirror reflectivity. For the case of reflection-mode operation [Fig. 1(b)], χ_r is a function of bottom mirror reflectivity only. χ_r-values close to one can be achieved for bottom mirror reflectivities higher than 0.99, which is easily obtained using DBR mirrors.

A. Inversion Level

It is desirable to operate an optical amplifier with a population inversion as high as possible in order to minimize reabsorption of the signal light, which is detrimental to the noise figure. The population inversion parameter is defined as [13]

$$n_{\rm sp} = \frac{N}{N-N_{\rm tr}} \tag{8}$$

where N is the carrier density and $N_{\rm tr}$ is the carrier density at transparency. $n_{\rm sp}$ takes on values greater than one for low carrier densities and reaches unity at complete inversion. A delicate problem inherent to FPAs is that strong pumping is desired to reach high carrier density, and thereby minimize $n_{\rm sp}$, while the amplifier still has to be operated in the regime below lasing

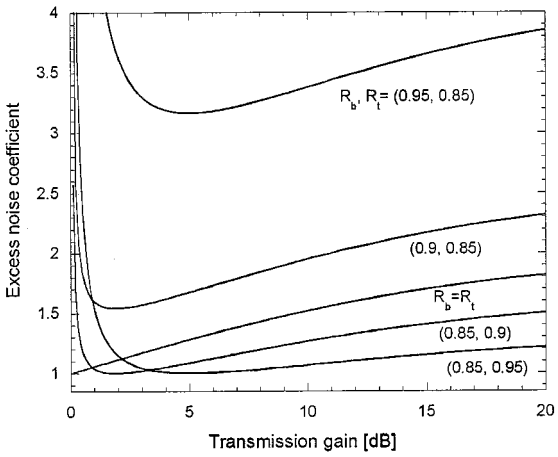

(a)

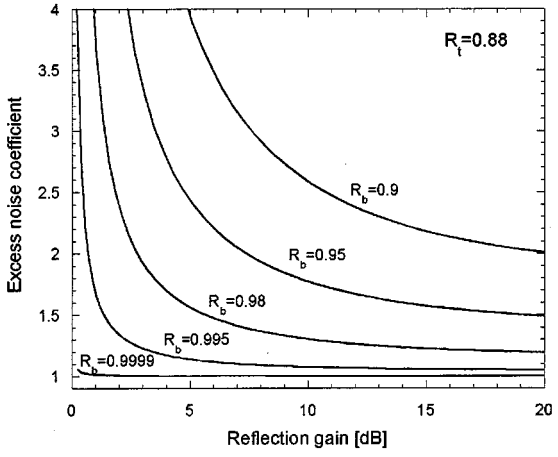

(b)

Fig. 1. Excess noise coefficient versus amplifier gain for: (a) transmission-mode operation and (b) reflection-mode operation.

threshold. The mirror reflectivity governs how hard the amplifier can be pumped before it reaches lasing threshold. Lasing threshold is reached when the round trip net gain equals one, i.e., $g_s^2 R_t R_b = 1$. The single-pass gain can be deduced from the active region design and the material gain, which is a function of carrier density. The population inversion can thus be linked to the single-pass gain and, if the reflectivities are known, the population inversion at threshold can be calculated. Fig. 2 shows a plot of the calculated population inversion parameter at threshold versus mirror reflectivity ($R_t \times R_b$) for the device described later in this paper. This marks the lowest possible value of $n_{\rm sp}$ for a given reflectivity; in practice, a VCSOA has to be operated at a slightly lower carrier density in order to avoid lasing. This particular device has an undoped InP–InGaAsP active region. The gain model for the device is described in [7]. The plot is valid for transmission or reflection-mode operation. For a reflection-mode device with bottom mirror reflectivity close to unity, the x-axis in the plot represents top mirror reflectivity. To achieve an $n_{\rm sp}$ below 1.5, the reflectivity has to be on the order of 0.9 or less. At low reflectivities and high carrier densities, changes in carrier density have a very small effect on the population inversion and values close to those given by the figure can be achieved. It has previously been shown that saturation output power and high gain-bandwidth product both

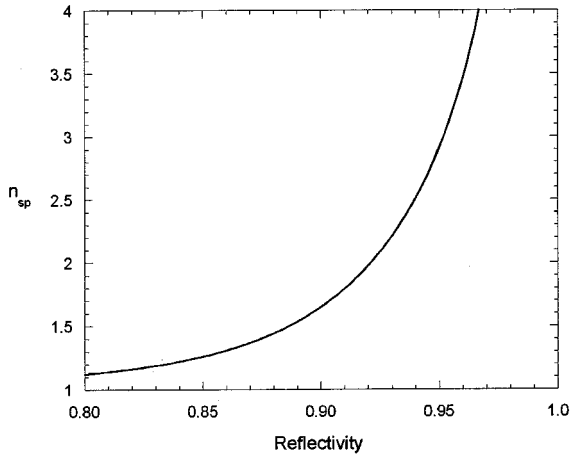

Fig. 2. Population inversion parameter versus reflectivity ($R_t \times R_b$) at lasing threshold.

benefit from low mirror reflectivity [2], [7]. It is clear from the discussion above that low mirror reflectivity is also crucial for achieving a low noise figure.

B. Coupling Efficiency

For any practical application, the often critical parameter is not the intrinsic noise figure of a device, but rather its fiber-to-fiber noise figure. The noise figure is degraded by loss associated with a coupling of signal into and out of the device. The fiber-to-fiber noise factor can be calculated using the equation for the noise factor of cascaded devices [16] as follows:

$$F_T = F_1 + \frac{F_2 - 1}{G_1} + \frac{F_3 - 1}{G_1 G_2} + \cdots. \tag{9}$$

The coupling losses can be modeled by attenuators with $\text{gain} = L < 1$ and noise figures $1/L$. For an amplifier with gain $G_{\rm amp}$ and intrinsic noise factor $F_{\rm amp}$, the total noise factor is then given by

$$F_T = \frac{F_{\rm amp}}{L_{\rm in}} + \frac{1}{G_{\rm amp} L_{\rm in} L_{\rm out}} - \frac{1}{G_{\rm amp} L_{\rm in}}. \tag{10}$$

This equation demonstrates that the input coupling loss directly degrades the noise factor (in logarithmic units, the input coupling loss is simply added to the noise figure), whereas the output coupling loss is only significant when the gain is small. VCSOAs have superior coupling efficiency compared to in-plane devices due to the circularly symmetric cross section of the optical mode. Coupling loss as low as 1 dB has been achieved for vertical-cavity lasers to single-mode fiber [17]. Similar output coupling efficiency could be achieved for a VCSOA; the input coupling efficiency should be even lower.

To summarize the theory, excess noise coefficients close to unity can be achieved, if the mirror reflectivities are chosen carefully (Fig. 1). High population inversion can also be obtained, using low mirror reflectivities and strong pumping (Fig. 2). This indicates that intrinsic noise figures close to 3 dB are possible to achieve. Assuming high gain and input coupling loss of less than 1 dB, fiber-to-fiber noise figures of about 4 dB should be possible for VCSOAs.

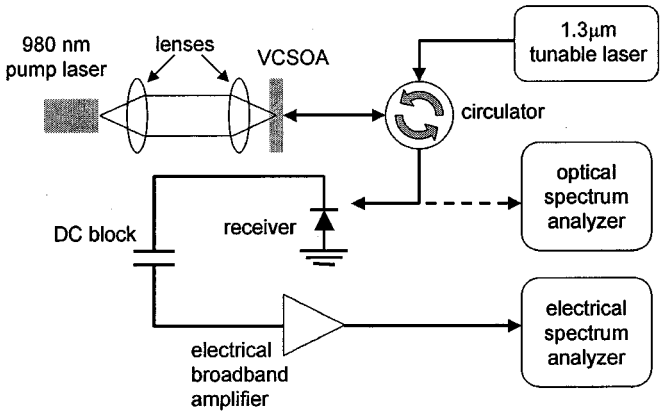

Fig. 3. Experimental setup.

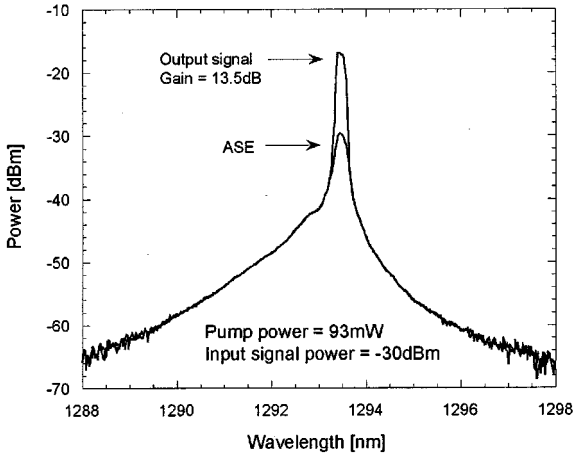

Fig. 4. Output spectra from 1.3-μm reflection-mode VCSOA. Output signal and ASE are shown for $P/P_{\rm th} = 0.9$ and -30-dBm input signal power.

III. Experiment

In order to verify the theory, noise figure measurements were performed on an optically pumped reflection-mode VCSAO operating at 1.3 μm. Both optical and electrical measurement techniques as described in [18] were used. The experimental setup is shown in Fig. 3. A Nortel 980-nm diode laser was used to pump the VCSOA. Free-space optics were used to focus the pump beam onto the device through the bottom DBR. An external cavity tunable laser diode was used as signal source. The signal was coupled into and out of the amplifier through a fiber and lens. The input and output signals were separated by means of an optical circulator. The total coupling loss, including the circulator was about 5 dB. A Hewlett-Packard optical spectrum analyzer was used for characterization of the optical spectrum of the output from the VCSOA. The electrical spectrum of the output was measured with a Rohde and Schwarz electrical spectral analyzer. A Nortel PP-10G p-i-n receiver was used to convert the optical signal. The detector was followed by a dc-block and a broadband SHF amplifier before the electrical spectral analyzer.

A detailed description of the structure of the VCSOA used in these experiments can be found in [2]. The device consists of a stacked multiple-quantum-well InGaAsP–InP active region wafer bonded to two GaAs–AlAs DBRs. Wafer bonding is described in [19]. The active region has three sets of seven quantum wells situated at the three central standing wave peaks in the 5/2λ-cavity. The bottom and top DBR has 25 and 13.5 periods, respectively. The device is a planar structure; the lateral dimensions of the active region are defined by the pump beam from the external pump laser, which was measured to be 8 μm. The reflectivity of the DBRs was calculated in order to estimate the possible noise figure of this device. For the bottom DBR, calculations were made based upon the number of mirror periods. The reflectivity was found to be 0.999. For the case of the top mirror, the reflectivity was deduced from gain bandwidth measurements. Equation (4) was fit to measured amplifier gain versus wavelength. The previously calculated reflectivity for the bottom mirror was used in the fit, which revealed a top mirror reflectivity of 0.955. An estimate of the possible noise figure can now be made based on the calculated mirror reflectivities and the previously presented design equations. Fig. 1(b) suggests an excess noise coefficient of 1, i.e., the bottom mirror reflectivity is high enough to not enhance the output noise from the amplifier. The lowest achievable population inversion parameter (at threshold) given by Fig. 2 is $n_{\rm sp} = 3$. These numbers inserted into (1) yield an intrinsic noise factor of $F = 6$, or $NF = 7.7$ dB. Assuming the input coupling loss to be about 1 dB, the best possible noise figure is $7.7{+}1 = 8.7$ dB.

Using optical measurement techniques, the noise figure is calculated from the spectral density of the ASE at the signal frequency, the amplifier gain and the energy of the signal photons. The noise factor in linear units is given by the following equation [18]:

$$F = \frac{2\rho_{\rm ase}}{Gh\nu} + \frac{1}{G}. \tag{11}$$

The first term represents signal-spontaneous beat noise and the second term represents shot noise. G is the amplifier gain, h is Planck's constant, ν is the frequency of the signal, and $\rho_{\rm ase}$ is the ASE density in the same polarization state as the signal. As the optical spectrum analyzer measures the total optical power in both polarization states, the factor $2\rho_{\rm ase}$ in (11) is simply replaced by the measured value. This method is only valid for small input signal powers when the ASE spectrum is unaffected by the signal. Spectra of the ASE and the output signal from the VCSOA, for the case of 93 mW of pump power (corresponding to $P/P_{\rm th} = 0.9$) and -30-dBm input signal are shown in Fig. 4. The measured fiber-to-fiber gain is 13.5 dB and the ASE is $2.78{*}10^{-17}$ W/Hz. This yields a fiber-to-fiber noise figure of 9.12 dB, calculated from (11). The value is in good agreement with the theoretical prediction. Deviations from the theoretical value can be attributed to the difficulties in measuring the ASE density over the small frequency interval of interest. The low-frequency noise, which is the most important part of the noise spectrum, is caused by beating with the ASE close to the signal frequency. For example, only beating with ASE components within a 20-GHz (0.11 nm) region around the signal frequency will show up in a 10-Gbit/s receiver. The spectrum analyzer has a resolution bandwidth of 0.1 nm. It is evident from the shape of the ASE spectrum (Fig. 4), the resolution of

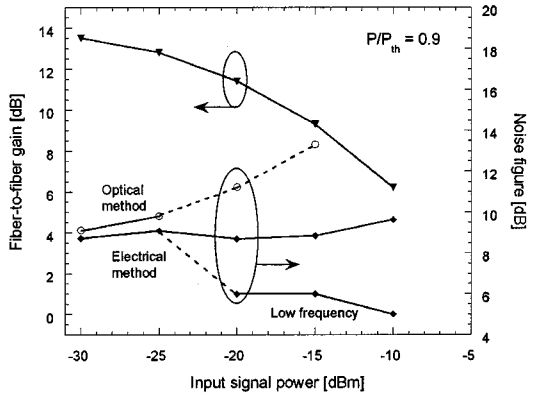

Fig. 5. Fiber-to-fiber gain and fiber-to-fiber noise figure versus input signal power for $P/P_{\rm th} = 0.9$.

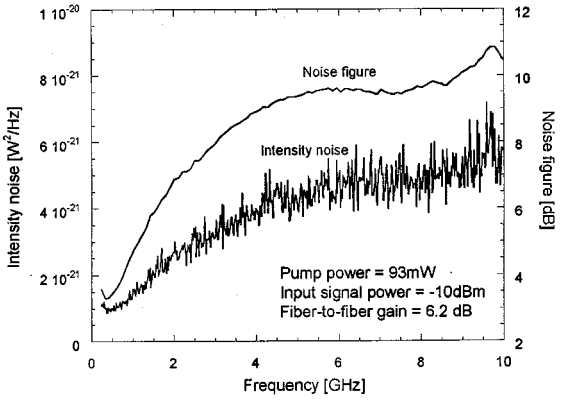

Fig. 6. Noise spectrum and noise figure for $P/P_{\rm th} = 0.9$ and -10-dBm input signal power.

the OSA, and the frequency range of interest that these measurements are associated with some uncertainty.

Electrical measurement techniques give a more complete characterization of the noise figure. The output noise from the amplifier is measured using a calibrated receiver and electrical spectrum analyzer. The thermal noise from the detector and shot noise is subtracted from the measured noise and an ideal shot noise term ($1/G$) is added. The noise figure is given by the following equation [18]:

$$F(f) = \frac{S_p(f)}{2h\nu G^2 P_{\rm in}} + \frac{1}{G} \tag{12}$$

where $S_p(f)$ is the measured and corrected electrical noise spectrum in W^2/Hz as a function of electrical frequency, and $P_{\rm in}$ is the input signal power. The input signal power was in the experiment controlled by means of a variable optical attenuator. The attenuation of the signal minimizes the excess noise of the signal that could otherwise affect the measurements. Noise spectra were measured from 0 to 10 GHz, for different input signal powers, and the noise figure was calculated using (12).

Noise figure and fiber-to-fiber gain for $P/P_{\rm th} = 0.9$ are shown in Fig. 5. Results from optical measurements are also shown in the figure. For low input signal power (-30 dB and -25 dB), gain of about 13 dB was measured. The noise figure given by the electrical method was about 9 dB. In this regime, the gain has not yet started to saturate and the gain and carrier density are unaffected by the input signal. The optical method is valid in this regime. The noise figure given by optical measurements is about 0.5 dB higher than that given by electrical measurements. For higher input signal powers, the optical method gives values that are too high, as the measured ASE density is higher than the ASE density when the signal is present. As the input signal power increases the amplifier gain starts to saturate. In this regime the carrier density in the QWs is depleted by the signal. The reduction in carrier density naturally causes a decrease in gain and yields an increased population inversion parameter. The decreased gain results in a power reduction of both output signal power and ASE power. The signal power, however, decreases faster resulting in degradation of the noise figure. It has been shown that at low electrical frequencies, the gain saturation causes a decrease in output noise resulting in a low-frequency noise figure considerably lower than the broad band noise figure [20]. The bandwidth of the low frequency dip in the noise spectrum is inversely proportional to the carrier lifetime and hence more significant in SOAs compared to fiber amplifiers [20]. A spectrum of the output noise and the noise figure for 93 mW of pump power and -10 dBm of signal is shown in Fig. 6. A noise figure smaller than 5 for frequencies below 1 GHz is demonstrated. The broadband noise figure is in this case about 10.

The measurements are, in general, in good agreement with theory. In the small signal regime, the measured noise figure of about 9 dB is close to the theoretical value of 8.7 dB. The deviation can be attributed to operation at slightly lower carrier density and uncertainties in the calculation of $n_{\rm sp}$, as well as in the estimate of the input coupling loss. The intrinsic noise figure of the present device trails those reported for in-plane devices [21], [22]. The superb coupling efficiency, however, yields an excellent fiber-to-fiber noise figure. The present device is clearly limited by a large population inversion parameter. Reduced mirror reflectivity would allow for stronger pumping and thereby a more favorable population inversion.

IV. Conclusion

We have investigated the noise figure of VCSOAs. Our initial results are promising; low noise figures can be expected from future devices. The noise figure is strongly affected by the reflectivity of the mirrors. The signal-spontaneous beat-noise enhancement (χ) can be eliminated by choosing proper mirror reflectivities. For the case of transmission-mode operation, low-input mirror reflectivity is desired in order to minimize χ. For reflection-mode operation, the bottom mirror reflectivity should be maximized to minimize χ, which for this case is independent of top mirror reflectivity. Highly reflective mirrors lead to lasing at relatively low carrier densities, which sets a limit to the possible population inversion. This is of more concern than the signal-spontaneous beat-noise enhancement. We have presented experimental results for the noise figure of a 1.3-μm VCSOA operated in reflection mode. The results are in good agreement with theory. The present devices have top mirror reflectivity (0.955) that is too high; the onset of lasing makes it impossible to achieve a population inversion below 3. Despite this, fiber-to-fiber noise figures on the order of 9 dB were measured. This clearly demonstrates that the superb coupling ef-

ficiency typical of vertical-cavity devices is advantageous for minimizing the fiber-to-fiber noise figure. Reduced mirror reflectivities on future devices will allow for stronger pumping, operation at higher carrier densities, and thereby a more favorable population inversion. The optimal design would be a transmission-mode device with input mirror reflectivity less than 0.85 and high output mirror reflectivity. Alternatively, a reflection-mode device with a top mirror reflectivity less than 0.9 and a bottom mirror reflectivity of >0.999 is desired. Noise figures close to the fundamental 3-dB limit can be expected in future devices.

REFERENCES

[1] D. Wiedenmann, C. Jung, M. Grabherr, R. Jäger, U. Martin, R. Michalzik, and K. J. Ebeling, "Oxide-confined vertical-cavity semiconductor optical amplifier for 980 nm wavelength," in *CLEO 98 Tech. Dig.*, 1998, Paper CThM5, p. 378.

[2] E. S. Bjorlin, B. Riou, P. Abraham, J. Piprek, Y.-J. Chiu, K. A. Black, A. Keating, and J. E. Bowers, "Long wavelength vertical-cavity semiconductor optical amplifiers," *IEEE J. Quantum Electron.*, vol. 37, pp. 274–281, Feb. 2001.

[3] R. Lewén, K. Streubel, A. Karlsson, and S. Rapp, "Experimental demonstration of a multifunctional long-wavelength vertical-cavity laser amplifier-detector," *IEEE Photon. Technol. Lett.*, vol. 10, pp. 1067–1069, 1998.

[4] N. Bouché, B. Corbett, R. Kuszelewicz, and R. Ray, "Vertical-cavity amplifying photonic switch at 1.5 μm," *IEEE Photon. Technol. Lett.*, vol. 8, pp. 1035–1037, 1996.

[5] C. Tombling, T. Saito, and T. Mukai, "Performance predictions for vertical-cavity semiconductor laser amplifiers," *IEEE J. Quantum Electron.*, vol. 30, pp. 2491–2499, Nov. 1994.

[6] A. Karlsson and M. Höijer, "Analysis of a VCLAD: Vertical-cavity laser amplifier detector," *IEEE Photon. Technol. Lett.*, vol. 7, pp. 1336–1338, Nov. 1995.

[7] J. Piprek, S. Björlin, and J. E. Bowers, "Design and analysis of vertical-cavity semiconductor optical amplifiers," *IEEE J. Quantum Electron.*, vol. 37, pp. 127–134, Jan. 2001.

[8] E. Desurvire, *Erbium-Doped Fiber Amplifiers, Principles and Applications*. New York: Wiley, 1994.

[9] H. Ghafouri-Shiraz, *Fundamentals of Laser Diode Amplifiers*. New York: Wiley, 1996.

[10] T. Mukai and Y. Yamamoto, "Noise in AlGaAs semiconductor laser amplifier," *IEEE J. Quantum Electron.*, vol. QE-18, pp. 564–575, Apr. 1982.

[11] K. Shimoda, H. Takahasi, and C. H. Townes, "Fluctuations in amplification of quanta with application to Maser amplifiers," *J. Phys. Soc. Jpn.*, vol. 12, pp. 686–700, June 1957.

[12] Y. Yamamoto, "Noise and error rate performance of semiconductor laser amplifiers in PCM-IM optical transmission systems," *IEEE J. Quantum Electron.*, vol. QE-16, pp. 1073–1081, Oct. 1980.

[13] T. Mukai, Y. Yamamoto, and T. Kimura, "S/N and error rate performance in AlGaAs semiconductor laser amplifier and linear repeater systems," *IEEE Trans. Microwave Theory Tech.*, vol. MTT-30, pp. 1548–1556, Oct. 1982.

[14] K. Hinton, "Model for noise processes in semiconductor laser amplifiers: Part 2," *Opt. Quant. Electron.*, vol. 23, pp. 755–773, 1991.

[15] T. Mukai, Y. Yamamoto, and T. Kimura, "Optical amplification by semiconductor lasers," in *Semiconductors and Semimetals*, R. K. Willardson and A. C. Beer, Eds. New York: Academic, 1985, vol. 22-E, pp. 265–319.

[16] R. S. Tucker and D. M. Baney, "Optical noise figure: Theory and measurements," in *OFC 2001 Tech. Dig.*, 2001, paper WI1.

[17] V. Jayaraman, J. Geske, M. McDougal, F. Peters, T. Lowes, T. Char, D. Van Deusen, T. Goodnough, M. Donhowe, S. Kilcoyne, and D. Welch, "Long-wavelength vertical-cavity laser research at Gore," in *Proc. SPIE*, vol. 3627, 1999, pp. 29–37.

[18] D. M. Baney, P. Gallion, and R. S. Tucker, "Theory and measurement techniques for the noise figure of optical amplifiers," *Opt. Fiber Technol.*, vol. 6, pp. 122–154, 2000.

[19] A. Black, A. R. Hawkins, N. M. Margalit, D. I. Babic, A. L. Jr. Holmes, Y.-L. Chang, P. Abraham, J. E. Bowers, and E. L. Hu, "Wafer fusion: Materials issues and device results," *IEEE J. Select. Topics Quantum Electron.*, vol. 3, pp. 943–951, 1997.

[20] M. Shtaif and G. Eisenstein, "Noise characteristics of nonlinear semiconductor optical amplifiers in the Gaussian limit," *IEEE J. Quantum Electron.*, vol. 32, pp. 1801–1809, Oct. 1996.

[21] T. Mukai and T. Saitoh, "5.2dB noise figure in a 1.5μm InGaAsP travelling-wave laser amplifier," *Electron Lett.*, vol. 23, pp. 216–217, Feb. 1987.

[22] A. E. Kelly, I. F. Lealman, L. J. Rivers, S. D. Perrin, and M. Silver, "Low noise figure (7.2dB) and high gain (29dB) semiconductor optical amplifier with a single layer AR coating," *Electron Lett.*, vol. 33, pp. 536–538, Mar. 1997.

E. Staffan Björlin (S'01) received the M.S. degree in engineering physics from the Royal Institute of Technology, Stockholm, Sweden, in 2000. He is currently working toward the Ph.D. degree in electrical engineering at the University of California at Santa Barbara.

His current research interests include design and analysis of vertical-cavity semiconductor optical amplifiers and their applications in optical communication systems.

John E. Bowers (S'78–M'81–SM'85–F'93) received the Ph.D. degree in applied physics from Stanford University, Stanford, CA.

He is the Director of the Multidisciplinary Optical Switching Technology Center (MOST), Executive Director of the Center for Entrepreneurship and Engineering Management, and a Professor in the Department of Electrical Engineering, all at the University of California at Santa Barbara. He has also worked for AT&T Bell Laboratories and Honeywell. His research interests are primarily concerned with optoelectronic devices and fiber optics. He has published six book chapters and over 400 papers.

Dr. Bowers is a Fellow of the American Physical Society and a recipient of the IEEE LEOS William Streifer Award.